Applied Catalysis B: Environmental 205 (2017) 631–636

Contents lists available at ScienceDirect

Applied Catalysis B: Environmental

journal homepage: www.elsevier.com/locate/apcatb

Optimization of defect distribution in photodegradation of air pollutants via SiO_2-shell-enhanced fluorine modification

Jinze Lyu[a,b,c,*], Junxian Gao[a], Min Zhang[a], Yanhong Wang[a], Dandan Hu[a], Juan Yi[a], Junbo Zhong[d], Ji Li[a], Shuo Wang[a]

[a] School of Environment and Civil Engineering, Jiangnan University, Wuxi, Jiangsu, 214122, China
[b] Jiangsu Key Laboratory of Anaerobic Biotechnology, Jiangnan University, Wuxi, Jiangsu, 214122, China
[c] Jiangsu College of Water Treatment Technology and Material Collaborative Innovation Center, Suzhou, Jiangsu, 215009, China
[d] Key Laboratory of Green Catalysis of Higher Education Institutes of Sichuan, College of Chemistry and Pharmaceutical Engineering, Sichuan University of Science and Engineering, Zigong, Sichuan, 643000, China

ARTICLE INFO

Article history:
Received 26 November 2016
Received in revised form 1 January 2017
Accepted 4 January 2017
Available online 5 January 2017

Keywords:
Catalytic
Surface defect
Bulk defect
Volatile organic compounds
Surface photovoltage

ABSTRACT

The distribution of bulk and surface defects significantly affects the separation and injection of photogenerated charge carriers. In this study, we provide a strategy of SiO_2-shell-enhanced F modification to optimize the distribution of bulk and surface defects. The effects of SiO_2 coating and F modification on the physical structure, the separation behavior of photogenerated charge carriers, and the photocatalytic activity of P25 were studied by transmission electron microscopy, X-ray diffraction, X-ray photoelectron spectroscopy, surface photovoltage spectroscopy, and toluene degradation experiments. Results showed that the removal rate of toluene over SiO_2-F-modified P25 was significantly higher than those over P25 and F modified P25. The SiO_2-shell-enhanced F modification simultaneously increased the content of surface Ti^{3+} and reduced the bulk defects, thereby enhancing the separation of charge carriers. Furthermore, F doped at surface exerted a strong catalytic effect on the removal of toluene, whereas F doped in lattice caused the recombination of photogenerated charge carriers. The SiO_2 coating and calcination treatment significantly increased the amount of F ions doped at TiO_2 surface and inhibited F doping in lattice.

1. Introduction

Photocatalysis is one of the most promising technologies for environmental pollution control, H_2 generation, and solar cells [1–4]. In recent years, photocatalytic technologies with TiO_2 as the major catalyst, such as degradation of volatile organic compounds (VOCs), were practically applied for environmental cleaning [5–7]. However, the related moderate photoactivity limits its practical application [8].

The photocatalytic process is simply divided into three steps, namely, generation of charge carriers (electrons and holes), migration from bulk to surface, and injection from catalyst to adsorbed species. The photogenerated electrons and holes easily recombine before being injected to an electron acceptor (e.g., O_2) and donor (e.g., organic species and hydroxyl), resulting in declined photoactivity. The photoactivity of a certain catalyst is mainly determined by the separation and injection efficiencies of charge carriers. A defect is the major site for recombination or injection of charge carriers, and its effect on catalyst photoactivity was theoretically or experimentally studied in many works [9–12]. Bulk defect is the major recombination center of charge carriers, and the effects of surface defects are highly complicated. Surface defects, such as Ti^{3+} and oxygen vacancy, increase the adsorption amount of O_2 or other reactants and thus enhance the injection of photogenerated electrons [13–15]. Surface defects are beneficial in constructing an electric field which drives photogenerated electrons and holes to separation toward the opposite direction in the near-surface region [16]. Surface defects also act as the recombination center of photogenerated charge carriers [17,18]. Generally, the photoactivity of a semiconductor catalyst decreases as the bulk defects increase, but it increases with surface defects in an appropriate scale. Several methods have been developed to control the amount of surface and bulk defects. Domen et al. created surface defects on $LaTiO_2N$ surface by using a brief aqua regia treatment to improve the photoactivity of the catalyst [19]. Chen et al. synthesized black TiO_2 by introducing a disorder in the surface region of TiO_2 through hydrogenation [20]. This material presents a large amount of sur-

* Corresponding author at: School of Environment and Civil Engineering, Jiangnan University, Wuxi, Jiangsu, 214122, China.
E-mail address: ljz@jiangnan.edu.cn (J. Lyu).

http://dx.doi.org/10.1016/j.apcatb.2017.01.012
0926-3373/

face defects and demonstrates excellent solar-driven photoactivity. Hydrogen thermal treatment, high energy particle bombardment, or thermal annealing under oxygen-depleted atmosphere was also used to create defects on catalyst surfaces [21,22]. However, surface oxygen vacancy is not stable and easily heals in the presence of O_2 and H_2O [10]. Several studies reported that F doping creates stable Ti^{3+} at the surface or subsurface and significantly enhances the photoactivity of catalysts [23–25]. The above methods efficiently increased surface defects but are unable to reduce the amount of bulk defects. Calcination at a relatively high temperature increases the crystallinity degree of catalysts and thus decreases the amount of bulk defects. Li et al. reported that the relative concentration ratio of surface to bulk defects of TiO_2 increases with the heating temperature, and the increased ratio of surface/bulk defects enhances photoactivity [26]. However, the calcination method also presents limitations. The absolute amount of surface defects is reduced during heating. Moreover, nanocrystals merge into larger ones as the heating temperature is increased, causing reduced surface area and unfavorable phase transformation. TiO_2 transforms from a relative high active phase (anatase) to a relative low active phase (rutile) at the temperature of >650 °C [27]. To our knowledge, few methods have been reported to optimize the distribution of surface and bulk defects without the above limitations.

In the current study, we proposed a SiO_2-shell-enhanced F modification strategy to simultaneously reduce bulk defects and increase surface defects of TiO_2 without reduction of surface area and unfavorable phase change. The effects of SiO_2 and F on physical properties, defect distribution, charge carrier separation behavior, and photoactivity were studied using high-resolution transmission electron microscopy (HRTEM), X-ray diffraction (XRD), X-ray photoelectron spectroscopy (XPS), surface photovoltage spectroscopy (SPS), and toluene degradation experiments.

2. Materials and methods

2.1. Catalyst preparation

Degussa P25 was used as model of TiO_2. SiO_2 shell was coated onto P25 nanoparticles by using the classic Stöber method [28]. For a typical synthesis, 0.75 g of P25, 70 mL of deionized water, and 5 mL of concentrated ammonia solution (28 wt%, Aladdin Chemistry, China) were added into 280 mL of absolute ethyl alcohol (99.5%, Aladdin Chemistry, China). Afterward, the mixture underwent ultrasonication for 15 min. Tetraethyl orthosilicate (2.4 mL, 99%, Aladdin Chemistry, China) was added dropwise to the dispersion of P25 particles for 10 min under continuous stirring, and the mixture was stirred at 25 °C for 18 h. Subsequently, the solution was centrifuged. The obtained solid was dried at 60 °C in an oven and calcined at 700 °C in furnace for 30 min. The obtained material was named as P25@SiO_2. Partial P25@SiO_2 was added to the HF solution (7 wt%) and stirred for 48 h to remove the SiO_2 shell and dope F at the catalyst surface. The mass ratio of P25@SiO_2 to HF solution was set to 1:30 to produce excessive F ions (the mole ratio of F:(Ti + Si) > 8). The solid was then washed with deionized water to remove the extra HF on the surface and was dried at 60 °C. The obtained SiO_2-F-modified sample was named P25@-F. A control material (P25-F) was synthesized following the same process, except for SiO_2 coating and calcination.

2.2. Photocatalytic experiment

Detailed information about the setups for the photocatalytic experiments was reported in our previous work [6,7]. The setups consist of a gas chamber, reactor, and gas chromatography (GC, 9790II, Fuli instrument, China) equipped with two flame ionization detectors and a methane converter, as shown in Fig. S1. An air pump with flow rate of 1 L/min was applied to circulate the air between the reactor and gas chamber. Another air pump with flow rate of 150 mL/min was used to circulate the air between the GC and gas chamber. The total volume of the whole system was 21.4 L. A quartz tube was placed in a dark box and surrounded by four UV lamps (8 W, Philips, central emission wavelength of 254 nm; the secondary wave at 183 nm was filtered) to complete the photocatalytic reactor. Briefly, 20 ± 0.1 mg of the prepared sample was dispersed in 10 mL of ethanol and coated on the inner face of a quartz tube by rotating in an oven. All quartz tubes were dried at 60 °C for 4 h before use. Highly pure air mixed with 79% N_2 and 21% O_2 (99.999%) was used to replace the gas in the system before each measurement. The initial relative humidity (RH) in the system was adjusted to 50% and detected by a humidity meter (DT-616CT, CEM, china). Toluene (99.5%, Aladdin Chemistry, China) was injected into the gas chamber until the toluene concentration in the system reaches up to 22 mg/m^3. Afterward, the gas in the chamber was switched to the reactor while simultaneously turning on UV light. The concentrations of toluene in the gas chamber were automatically detected by GC every 8 min. All measurements were repeated thrice.

2.3. Characterization of catalysts

A N_2 adsorption/desorption isotherm was detected using an Autosorb-iQ2-MP Surface Area Analyzer (Quantachrome, USA). The crystal pattern and crystal size were measured by XRD (D8 Advance, Bruker, Germany) with Cu Kα radiation ($\Delta 2\theta = 0.02°$, $\lambda = 0.15406$ nm). The morphology of the prepared samples was observed through HRTEM (JEM-2100, JEOL, Japan) at an accelerating voltage of 200 kV. The valence of the surface elements of the samples was analyzed by XPS (PHI Quantera II, Japan) with Al-Kα as X-ray source. The pressure of the XPS system was set to 6×10^{-6} Pa before the test. Each XPS curve was calibrated by an adventitious carbon signal at 284.6 eV. The separation efficiency and transfer direction of photogenerated charge carriers were estimated by an assembled SPS system. The system consists of a xenon lamp (500 W, LSB-X500, Zolix, China), a monochromator (Omni-λ300, Zolix, China), a light chopper (SR540, Stanford Research Systems, USA), a photovoltaic cell, a lock-in amplifier (SR830, Stanford Research Systems, USA), and a computer (Fig. S2). The samples were contacted with an upper ITO glass and a Cu base in the photovoltaic cell. The light from the monochromator was chopped to 23 Hz, and the prepared samples were irradiated through the upper ITO glass. The scanned monochromatic light began at 500 nm and ended at 300 nm. The RH and temperature in the room where the SPS system is located were set constant at 50% and 25 °C, respectively. Other details of the SPS system were reported in our previous works [6,7].

3. Results and discussion

3.1. TEM measurement

The micromorphology of the prepared samples was observed using HRTEM. Fig. 1A shows that P25 consists of nanoparticles with an average size of approximately 23 nm. SiO_2 was successfully coated on the P25 particles and formed a uniform shell, as shown Fig. 1B. The thickness of the SiO_2 shell for P25@SiO_2 was approximately 19.3 nm. After the SiO_2 shell was etched with HF solution, the exposed inner TiO_2 nanoparticle, P25@-F, exhibited shape and size similar to those of P25 (average 24 nm, Fig. 1C). TiO_2 particles combined into larger ones, accompanied by crystal phase transformation from anatase to rutile as the heating temperature

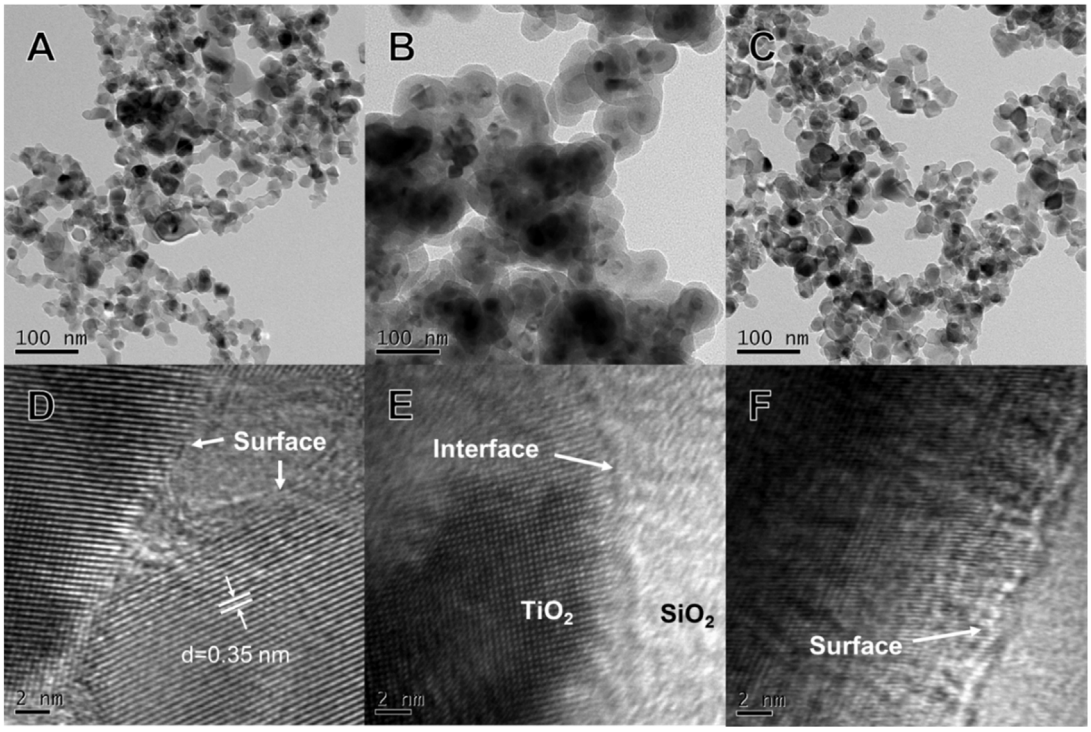

Fig. 1. Transmission electron microscopy images of P25 (A, D), P25@SiO_2 (B, E), and P25@-F (C, F).

was >650 °C [27]. However, TiO_2 particles maintained their original size after heating at 700 °C in the presence of the SiO_2 shell. Moreover, anatase TiO_2 (101) facets exist with distinct lattice fringes of d = 0.35 nm are the most commonly observed facets in the HRTEM images of P25@SiO_2 and P25@-F (Fig. 1E and F). This finding suggested that SiO_2 shell with 19.3 nm thick also restricts the phase transformation of inner TiO_2 particles. Fig. 1D and E shows that the ordered lattice fringes of P25 and P25@SiO_2 stopped close to the surface and thus formed a relatively clear surface edge. However, after the treatment of HF solution, the lattice fringes became ambiguous in the near-surface region, as shown in Fig. 1F. These results revealed that the doped F created a number of defects at the catalyst surface. Different from P25 and P25@SiO_2, some dark dots were observed in the HRTEM image of P25@-F. The dark dots appeared because doped F changed the local state density. Similar F corroded layer was observed in the HRTEM image of P25-F, as shown in Fig. S3. However, the particle size of P25-F is larger (average 42.8 nm) and the rutile (001) facet is more exposed with lattice fringes of d = 0.24 nm than those of P25@-F. This finding revealed that HF created defects in the near-surface region of P25, rearranged the Ti and O atoms in bulk, and formed larger nanoparticles with higher proportion of rutile pattern without SiO_2 coating and calcination. Given this finding, calcination in the presence of SiO_2 shell significantly enhanced the stability of inner TiO_2 particles.

3.2. N_2 adsorption and desorption measurement

N_2 adsorption–desorption experiments were conducted to estimate the structure of the prepared samples. Brunauer–Emmett–Teller method [29] was used to calculate the specific surface area (S_{BET}). Barrett–Joyner–Halenda method [30] was applied to estimate the average pore size. Table 1 shows the summary of S_{BET}, pore volume, and average pore size of the prepared samples. The S_{BET} of P25@-F revealed no obvious difference with P25. This finding further proved that the merging of inner TiO_2 particles at 700 °C was inhibited by the coated SiO_2 shell,

Table 1
Structural properties of the prepared nanocatalysts.

Samples	S_{BET} (m^2/g)	Total volume (cm^3/g)	Average pore size (nm)
P25	50.5	0.160	12.2
P25-F	48.8	0.141	12.1
P25@-F	49.8	0.155	12.4

which agrees with the TEM results. The total pore volume and S_{BET} were slightly reduced without SiO_2 coating and calcination treatment. The surface area is a key parameter that significantly affects the photoactivity of catalysts. The effect of surface area should show no obvious difference on the photocatalytic activity of the prepared samples with similar S_{BET}.

3.3. XRD measurement

TEM and N_2 adsorption–desorption measurements showed that SiO_2 shell inhibited the change of inner P25 particles in shape, size, and surface area. We further conducted XRD measurement to study the effect of SiO_2 coating and calcination treatment on the crystal structure of the inner TiO_2 particles. Fig. 2 shows that the peaks of the prepared samples are indexed to the identical crystal planes of anatase TiO_2 and rutile TiO_2, revealing that all samples exhibited the mixed crystal phase of anatase and rutile. The intensity of anatase peaks was reduced, whereas that of rutile peaks was increased with direct HF treatment compared with P25. This finding revealed that HF treatment transformed a part of the anatase pattern to rutile pattern in P25. However, after SiO_2 coating and calcination, HF did not obviously change the crystal pattern of the inner TiO_2. The crystal size of P25 was 20 nm, similar to the particle size obtained in Fig. 1A. After SiO_2 coating and F doping, the crystal size of inner TiO_2 was reduced to 18.4 nm. However, the particle size of P25@-F was not reduced compared with P25, as shown in Fig. 1A and C. Given Fig. 1F, the crystal size was reduced because of the defects induced by F doping in the near-surface region. The intensity of XRD peaks indexed the crystallinity of the samples.

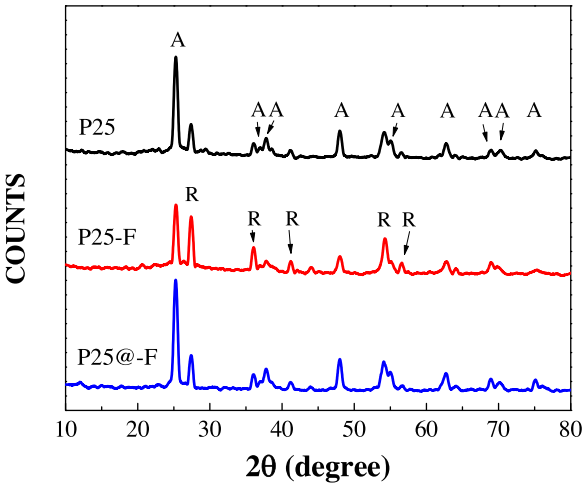

Fig. 2. XRD patterns of P25, P25-F, and P25@-F.

Fig. 2 shows that the intensity of P25@-F peaks, both for rutile and anatase peaks, was slightly higher than that of P25. Given that F doping created a certain amount of defects in the near-surface region of P25@-F, the increase in XRD peaks was derived from the bulk of P25@-F. This finding proved that the bulk defects of the inner TiO_2 were obviously reduced by calcination in the presence of SiO_2 shell. By contrast, P25-F exhibited a relatively low peak intensity, revealing that direct HF treatment significantly reduced the crystallinity of P25. Above all, the SiO_2-shell-enhanced F modification simultaneously increased the F-induced surface defects and reduced the bulk defects without obviously changing the size, shape, surface area, and crystal pattern of inner TiO_2 particles. Photocatalytic activity is usually increased with the degree of crystallinity because of the few bulk defects and low number of $e^- - h^+$ pair recombination [31]. On the contrary, surface defects are the major catalytic sites and are beneficial for the separation of photogenerated charge carriers [15,16]. These findings indicated that P25@-F with optimized distribution of surface and bulk defects exhibits outstanding photoactivity.

3.4. Characterization of the surface elements on the catalyst surface

XPS measurements were conducted to study the effects of SiO_2 coating and F modification on the chemical state of the surface elements. Fig. S4 shows no Si peak observed in the whole XPS spectra of P25@-F, indicating that SiO_2 shell was thoroughly removed by the HF solution. Therefore, the effect of Si on the reaction property of P25@-F surface was excluded. The peaks at 684 and 689 eV were assigned to F 1 s orbital for F at the surface and in the lattice, respectively [32,33]. Fig. 3A shows that P25-F possesses both surface F and lattice F, whereas P25@-F exhibits only F at the surface. TEM and XRD results proved that direct HF treatment caused phase transformation and aggregation of TiO_2 nanocrystals. Therefore, in the direct HF treatment, F ions were doped into the lattice of TiO_2 during the rearrangement of Ti and O atoms. Golovko et al. treated P25 with six different F-containing surface modifying agents [34]. The double peaks of surface and lattice F were observed in the XPS spectra of all F-modified samples. This finding suggested that F was easily doped to the lattice of P25. However, in this work, F doping in lattice was inhibited after SiO_2 coating and calcination. We further calculated the area ratio of surface F1s peak at 684 eV to Ti2p peak at 458.4 eV to estimate the relative content of surface F. The F/Ti peak ratio of P25@-F was 0.155, which was 3.5 times higher than that of P25-F. This finding proved that the SiO_2 coating and

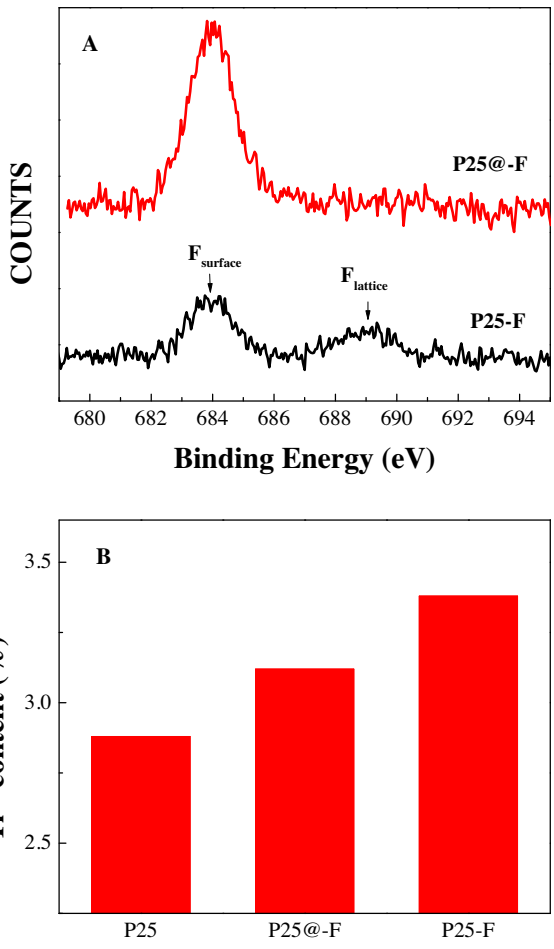

Fig. 3. F1s XPS (A) and Ti^{3+} content (B) of the prepared samples.

calcination inhibited F doping into the TiO_2 lattice and increased the content of F doped at surface. The peaks at 457.4 and 458.4 eV were assigned to Ti^{3+} and Ti^{4+}, respectively [35]. These findings indicated that the Ti2p peaks of the prepared samples in the present research were deconvolved on the basis of the Ti^{3+} and Ti^{4+} peaks in the abovementioned study, as shown in Fig. S4. Fig. 3B shows the content of Ti^{3+} for the prepared samples in the following order: P25-F > P25@-F > P25. Doped F ions created a Ti^{3+} site by transferring electrons to the adjacent Ti^{4+} [32]. Compared with P25, the increased Ti^{3+} was located at the surface or subsurface because F ions were only doped at the P25@-F surface. P25-F presented less surface F but more lattice F; therefore, the increased Ti^{3+} for P25-F was mostly present in bulk rather than at the surface. Li et al. stated that the photoactivity of catalysts increases with the ratio of surface defects and bulk defects [26]. Surface defects comprise the active photocatalytic center, whereas bulk defects act as the major recombination center of photogenerated charge carriers [36–39]. According to the XPS and XRD results, the SiO_2-shell-enhanced F modification presented in this work efficiently and simultaneously increased the surface defects and reduced the bulk defects. Hence, the redistribution of bulk and surface defects should enhance the charge-separation efficiency.

3.5. Photocatalytic degradation of toluene

No obvious change in toluene concentration was detected in the control experiments without photocatalysts or UV light irradiation. Fig. 4 shows the reduced rate of toluene concentration in the following order: P25@-F > P25-F > P25. P25@-F reduced the

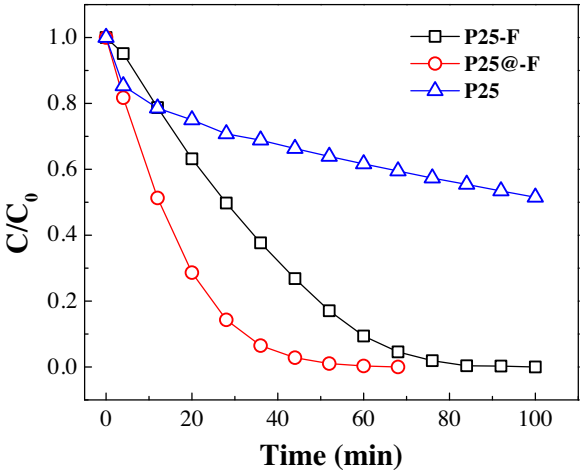

Fig. 4. Removal curves of toluene over the prepared samples (C_0 is the initial concentration of toluene in gas chamber, 22 mg/m^3; C is the toluene concentration in gas chamber in different times).

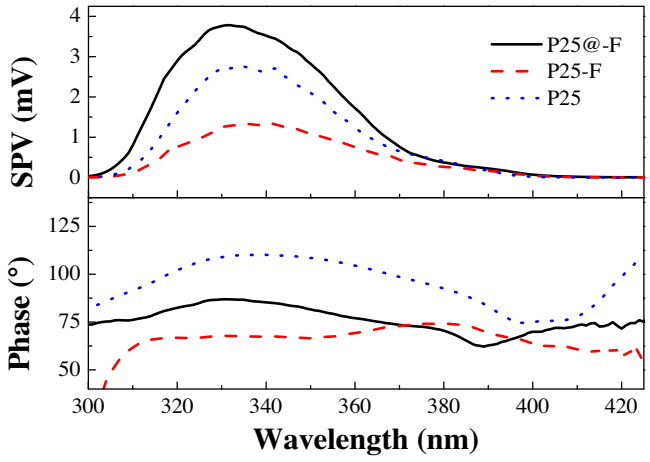

Fig. 5. Surface photovoltage and phase spectra of the prepared samples.

toluene concentration quicker than P25 and P25-F did. P25 required 364 min to reduce toluene to an undetectable concentration, whereas P25-F required only 84 min. P25@-F further shortened the degradation time to 60 min. The outstanding performance of P25@-F in toluene removal can easily be understood by the optimized defect distribution and F doping. The removal of toluene over P25-F showed specific information. According to the XRD and XPS results, direct HF treatment induced a certain amount of bulk defects, which will lead to the recombination of photogenerated charge carriers. Therefore, the relatively high removal rate of toluene over P25-F was a positive effect of doped F ions. F doping exerts two major positive effects on the photocatalytic process, namely, enhancing the separation of photogenerated charge carriers [40] and catalyzing surface reactions [23]. To further evaluate the effect of F doping on the photocatalytic process, we studied the charge-separation behavior by using SPS technology.

3.6. Separation behavior of photogenerated charge carriers at the catalyst surface

SPS is a handy tool for studying the separation behavior of photogenerated charge carriers. The intensity of surface photovoltage (SPV) signal reflects the separation efficiency of photogenerated charge carriers. The corresponding phase spectrum indicates the band bending direction and the charge transfer trend. As the phase is controlled by many carrier transfer processes, discussing the phase spectra around bandgap is recommended. Generally, the phase shifts toward ±0° (±180°) in the case of upward band bending (downward band bending) as the light *hv* increases around the bandgap; the trend of holes (electrons) migrating to the catalyst surface increases as the |phase| is reduced (increased) [41,42]. Fig. 5 shows the SPV of the prepared samples in the following order: P25@-F > P25 > P25-F. The SPV of P25@-F was 3.8 mV, 1.4 and 2.8 times higher than that of P25 and P25-F, respectively. This finding explains that SiO_2-shell-enhanced F modification significantly enhanced the separation efficiency of charge carriers, whereas direct HF treatment reduced the efficiency. The XRD and TEM results proved that calcination in the presence of SiO_2 shell efficiently reduced the bulk defects and thus reduced the recombination center of charge carriers. Moreover, F-induced Ti^{3+} was located at the surface or subsurface region of P25@-F after SiO_2 coating and calcination treatment. However, F was doped in TiO_2 lattice and thus created additional bulk defects during direct HF treatment. Given the high electric resistance of TiO_2, these bulk defects cannot enhance the adsorption of reactants, such as O_2, and thus act only as the recombination center of photogenerated charge carriers. This phenomenon explains why direct HF treatment reduced the charge-separation efficiency. Interestingly, P25-F with a lower charge-separation efficiency showed higher removal rate of toluene compared with P25, as shown in Fig. 4. Zhao and Chen recently reported that the first-layer water at TiO_2 surface is possibly adsorbed in a dual H-bonding mode on adjacent surface F sites, thereby kinetically facilitating the cleavage of O—H bonds by proton-coupled electron transfer [23]. Liew and Liu stated that doped F on anatase TiO_2 surface promotes the adsorption ability of catalyst surface for oxidative gas molecules, which is beneficial for separation and injection of charge carriers [40]. Given our experimental results, F doping at TiO_2 surface dominantly promoted the removal rate of toluene for P25-F by catalyzing the surface reaction rather than enhancing the charge separation.

Fig. 5 shows that the phase of P25 and P25@-F shifted to 180°, whereas the phase of P25-F revealed the opposite trend as the light *hv* increased around the bandgap. This result revealed that the energy band of P25 and P25@-F bended downward, whereas P25-F revealed upward band bending. Furthermore, both the phases of P25@-F and P25-F were lower than that of P25. The SPS signal generated by the light of wavelength of <370 nm majorly corresponded to the band-to-band electron excitation. Therefore, the phase result explains that the F doping enhanced the migration trend of holes toward the catalyst surface. O_2 and H_2O are the major substances in atmosphere that affect the near-surface electronic field of catalysts. H_2O directly adsorbs to neutral and perfect TiO_2 surface, whereas O_2 only adsorbs on the TiO_2 surface with surface (subsurface) oxygen vacancy or excess electron [37]. Adsorbed O_2 acts as electron acceptor and thus leads to the accumulation of electrons on the surface, whereas adsorbed H_2O and OH act in the opposite way [39]. Photogenerated holes (electrons) driven by the electronic field from the adsorbed O_2 (H_2O) are likely to migrate toward the catalyst surface. F doped at TiO_2 surface enhances the adsorption of O_2 and other oxidative gases [40]. With more O_2 adsorbed at surface, the electronic field built by the adsorbed gas enhanced the migration of photogenerated holes to the surface of F doped TiO_2.

Considering the above statements, we drew an illustration to explain the effects of the SiO_2 coating and F modification on the separation behavior of photogenerated charge carriers and surface reaction, as shown in Fig. 6. P25 with few surface defects was dominated by H_2O molecules and OH, thereby facilitating photogenerated electrons migration to the surface. After the SiO_2 coating and F modification, the bulk defects of inner TiO_2 was reduced, whereas surface Ti^{3+} was increased compared with P25, and a

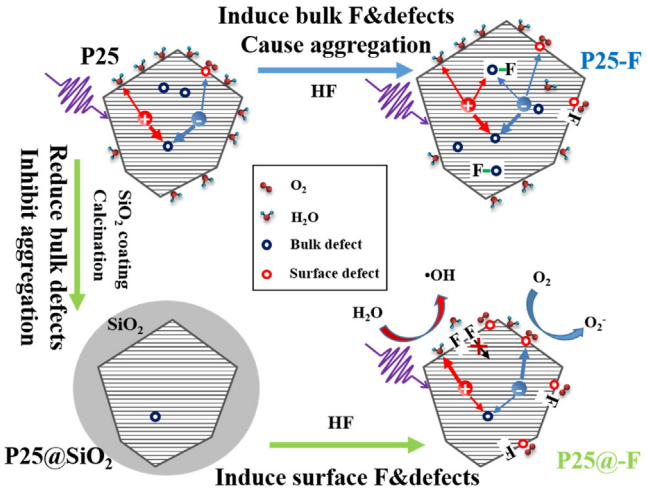

Fig. 6. The effects of synthetic strategies on the structure of the prepared samples and the corresponding separation behavior of charge carriers.

certain number of F ions were doped at the catalyst surface. The reduced bulk defects significantly decreased the recombination of photogenerated charge carriers. The doped F at TiO_2 surface acted as a catalytic site, which obviously enhanced the removal rate of toluene. Moreover, the doped F and newly formed surface Ti^{3+} enhanced the adsorption of O_2 molecules and thus changed the electric field in the near-surface region. Driven by the electric field, the migration of photogenerated holes to the catalyst surface was enhanced.

4. Conclusion

A new strategy of SiO_2-shell-enhanced F modification was applied to enhance the photoactivity of TiO_2 for photocatalytic removal of VOCs. After SiO_2-shell-enhanced F modification, the removal rate of toluene over the newly formed catalyst, P25@-F, significantly increased compared with P25 and F modified TiO_2 (P25-F). This result is mainly attributed to two reasons: 1) calcination in the presence of SiO_2 shell reduced the amount of bulk defects of inner TiO_2, thereby reducing the recombination of photogenerated charge carriers; and 2) after SiO_2 coating and calcination treatments, the content of F doped at the catalyst surface obviously increased, whereas F doping in lattice was inhibited. The surface doped F acted as a strong catalytic site and thus significantly enhanced the removal of toluene.

Acknowledgements

Financial support by Jiangsu Province Science Foundation for Youth (BK20150126), the Opening Project of Key Laboratory of Green Chemistry of Sichuan Institutes of Higher Education (LZJ14203), Fundamental Research Funds for the Central Universities (JUSRP51512), and Jiangnan University Science Foundation (JUSRP11522) is greatly appreciated.

Appendix A. Supplementary data

Supplementary data associated with this article can be found, in the online version, at http://dx.doi.org/10.1016/j.apcatb.2017.01.012.

References

[1] L. Ren, Y.Z. Li, J.T. Hou, J.L. Bai, M.Y. Mao, M. Zeng, X.J. Zhao, N. Li, Appl. Catal. B-Environ. 181 (2016) 625–634.
[2] D. Kim, D.R. Whang, S.Y. Park, J. Am. Chem. Soc. 138 (2016) 8698–8701.
[3] X. Chen, Q. Liu, Q.L. Wu, P.W. Du, J. Zhu, S.Y. Dai, S.F. Yang, Adv. Funct. Mater. 26 (2016) 1719–1728.
[4] X.F. Qian, D.T. Yue, Z.Y. Tian, M. Reng, Y. Zhu, M. Kan, T.Y. Zhang, Y.X. Zhao, Appl. Catal. B-Environ. 193 (2016) 16–21.
[5] N. Costarramone, B. Kartheuser, C. Pecheyran, T. Pigot, S. Lacombe, Catal. Today 252 (2015) 35–40.
[6] J. Lyu, J. Gao, M. Zhang, Q. Fu, L. Sun, S. Hu, J. Zhong, S. Wang, J. Li, Appl. Catal. B: Environ. 202 (2017) 664–670.
[7] J. Lyu, L. Sun, J. Zhong, Q. Fu, M. Zhang, S. Wang, J. Li, Chem. Eng. J. 303 (2016) 314–321.
[8] J. Lyu, L. Zhu, C. Burda, Catal. Today 225 (2014) 24–33.
[9] X.Y. Pan, M.Q. Yang, X.Z. Fu, N. Zhang, Y.J. Xu, Nanoscale 5 (2013) 3601–3614.
[10] S. Wendt, P.T. Sprunger, E. Lira, G.K.H. Madsen, Z.S. Li, J.O. Hansen, J. Matthiesen, A. Blekinge-Rasmussen, E. Laegsgaard, B. Hammer, F. Besenbacher, Science 320 (2008) 1755–1759.
[11] H.H. Pham, L.W. Wang, Phys. Chem. Chem. Phys. 17 (2015) 541–550.
[12] J. Lyu, L. Zhu, C. Burda, Chemcatchem 5 (2013) 3114–3123.
[13] C.L. Muhich, Y. Zhou, A.M. Holder, A.W. Weimer, C.B. Musgrave, J. Phys. Chem. C 116 (2012) 10138–10149.
[14] T. Tachikawa, Y. Takai, S. Tojo, M. Fujitsuka, T. Majima, Langmuir 22 (2006) 893–896.
[15] E. Lira, S. Wendt, P.P. Huo, J.O. Hansen, R. Streber, S. Porsgaard, Y.Y. Wei, R. Bechstein, E. Laegsgaard, F. Besenbacher, J. Am. Chem. Soc. 133 (2011) 6529–6532.
[16] Z. Zhang, J.T. Yates, Chem. Rev. 112 (2012) 5520–5551.
[17] K. Zhu, T.B. Vinzant, N.R. Neale, A.J. Frank, Nano Lett. 7 (2007) 3739–3746.
[18] X.B. Zhang, H.M. Tian, X.Y. Wang, G.G. Xue, Z.P. Tian, J.Y. Zhang, S.K. Yuan, T. Yu, Z.G. Zou, Mater. Lett. 100 (2013) 51–53.
[19] M. Matsukawa, R. Ishikawa, T. Hisatomi, Y. Moriya, N. Shibata, J. Kubota, Y. Ikuhara, K. Domen, Nano Lett. 14 (2014) 1038–1041.
[20] X.B. Chen, L. Liu, P.Y. Yu, S.S. Mao, Science 331 (2011) 746–750.
[21] E. Ioannidou, A. Ioannidi, Z. Frontistis, M. Antonopoulou, C. Tselios, D. Tsikritzis, I. Konstantinou, S. Kennou, D.I. Kondarides, D. Mantzavinos, Appl. Catal. B-Environ. 188 (2016) 65–76.
[22] Y.Z. Li, J.Y. Yu, W. Li, G.L. Fan, L. Yang, F. Li, Phys. Chem. Chem. Phys. 18 (2016) 6548–6558.
[23] H. Sheng, H.N. Zhang, W.J. Song, H.W. Ji, W.H. Ma, C.C. Chen, J.C. Zhao, Angew. Chem. Int. Ed. 54 (2015) 5905–5909.
[24] W.Q. Fang, X.L. Wang, H.M. Zhang, Y. Jia, Z.Y. Huo, Z. Li, H.J. Zhao, H.G. Yang, X.D. Yao, J. Mater. Chem. A 2 (2014) 3513–3520.
[25] C. Minero, G. Mariella, V. Maurino, E. Pelizzetti, Langmuir 16 (2000) 2632–2641.
[26] M. Kong, Y.Z. Li, X. Chen, T.T. Tian, P.F. Fang, F. Zheng, X.J. Zhao, J. Am. Chem. Soc. 133 (2011) 16414–16417.
[27] J. Zhang, M.J. Li, Z.C. Feng, J. Chen, C. Li, J. Phys. Chem. B 110 (2006) 927–935.
[28] W. Li, J.P. Yang, Z.X. Wu, J.X. Wang, B. Li, S.S. Feng, Y.H. Deng, F. Zhang, D.Y. Zhao, J. Am. Chem. Soc. 134 (2012) 11864–11867.
[29] S. Brunauer, P.H. Emmett, E. Teller, J. Am. Chem. Soc. 60 (1938) 309–319.
[30] E.P. Barrett, L.G. Joyner, P.P. Halenda, J. Am. Chem. Soc. 73 (1951) 373–380.
[31] V. Puddu, H. Choi, D.D. Dionysiou, G.L. Puma, Appl. Catal. B-Environ. 94 (2010) 211–218.
[32] A.M. Czoska, S. Livraghi, M. Chiesa, E. Giamello, S. Agnoli, G. Granozzi, E. Finazzi, C. Di Valentin, G. Pacchioni, J. Phys. Chem. C 112 (2008) 8951–8956.
[33] J.C. Yu, J.G. Yu, W.K. Ho, Z.T. Jiang, L.Z. Zhang, Chem. Mater. 14 (2002) 3808–3816.
[34] J.-Y. Ruzick, F. Abu Bakar, L. Thomsen, B.C. Cowie, C. McNicoll, T. Kemmitt, H.E.A. Brand, B. Ingham, G.G. Andersson, V.B. Golovko, RSC Adv. 4 (2014) 20649–20658.
[35] S. Rtimi, S. Giannakis, M. Bensimon, C. Pulgarin, R. Sanjines, J. Kiwi, Appl. Catal. B-Environ. 191 (2016) 42–52.
[36] M.A. Henderson, W.S. Epling, C.L. Perkins, C.H.F. Peden, U. Diebold, J. Phys. Chem. B 103 (1999) 5328–5337.
[37] C.L. Muhich, Y. Zhou, A.M. Holder, A.W. Weimer, C.B. Musgrave, J. Phys. Chem. C 116 (2012) 10138–10149.
[38] Q. Wu, R. van de Krol, J. Am. Chem. Soc. 134 (2012) 9369–9375.
[39] A. Stevanovic, M. Buttner, Z. Zhang, J.T. Yates, J. Am. Chem. Soc. 134 (2012) 324–332.
[40] H. Liu, K.M. Liew, C. Pan, RSC Adv. 4 (2014) 35928–35942.
[41] T. Ivanov, V. Donchev, K. Germanova, K. Kirilov, J. Phys. D-Appl. Phys. 42 (2009).
[42] V. Donchev, K. Kirilov, T. Ivanov, K. Germanova, Mater. Sci. Eng. B-Solid State Mater. Adv. Technol. 129 (2006) 186–192.